Available online at www.sciencedirect.com
SCIENCE DIRECT
Journal of Catalysis 234 (2005) 172–181
JOURNAL OF CATALYSIS
www.elsevier.com/locate/jcat

Model catalyst studies of the strong metal–support interaction: Surface structure identified by STM on Pd nanoparticles on TiO_2(110)

Michael Bowker [a,*], Peter Stone [b], Peter Morrall [b,1], Rupert Smith [b,2], Roger Bennett [b], Neil Perkins [b,3], Ren Kvon [c], Chi Pang [b], Elodie Fourre [a], Matthew Hall [a]

[a] *Surface Science and Catalysis Group, School of Chemistry, Cardiff University, Cardiff, CF10 3TB, UK*
[b] *Centre for Surface Science and Catalysis, School of Chemistry, University of Reading, Reading, RG6 6AD, UK*
[c] *Boreskov Catalysis Research Institute, Novosibirsk, Russia*

Received 9 February 2005; revised 24 May 2005; accepted 26 May 2005

Available online 19 July 2005

Abstract

Model catalysts of Pd nanoparticles and films on TiO_2(110) were fabricated by metal vapour deposition (MVD). Molecular beam measurements show that the particles are active for CO adsorption, with a global sticking probability of 0.25, but that they are deactivated by annealing above 600 K, an effect indicative of SMSI. The Pd nanoparticles are single crystals oriented with their (111) plane parallel to the surface plane of the titania. Analysis of the surface by atomic resolution STM shows that new structures have formed at the surface of the Pd nanoparticles and films after annealing above 800 K. There are only two structures, a zigzag arrangement and a much more complex "pinwheel" structure. The former has a unit cell containing 7 atoms, and the latter is a bigger unit cell containing 25 atoms. These new structures are due to an overlayer of titania that has appeared on the surface of the Pd nanoparticles after annealing, and it is proposed that the surface layer that causes the SMSI effect is a mixed alloy of Pd and Ti, with only two discrete ratios of atoms: Pd/Ti of 1:1 (pinwheel) and 1:2 (zigzag). We propose that it is these structures that cause the SMSI effect.

Keywords: SMSI; Strong metal–support interaction; Pd nanoparticles; CO adsorption; STM

1. Introduction

The SMSI effect was first described in 1978 by Tauster [1–4]. The effect was observed as a severely negative effect on CO and H_2 uptake on the catalyst after high-temperature calcinations (above about 700 K) [1,2]. It also has a negative effect on the reaction rate for reactions such as alkane hydrogenolysis [5,6]. From that early work it appeared that the effect occurred for catalysts comprising reducible supports and treated at elevated temperature in reducing conditions [2–4]. A classic support that has manifested this behaviour in many studies is TiO_2. Over the years after the first discovery of SMSI it has been recognised that the effect is not always negative—for instance, it appears to have a positive effect on the CO–H_2 reaction [5,6]. Furthermore, it was noted that hydrogen reduction was not necessary to observe the effect of CO adsorption suppression, it also occurs by vacuum treatment [7], though it should be noted that vacuum treatment at elevated temperature is, in effect, a reducing environment.

A number of models have been proposed to explain this phenomenon, but there are two main proposals: that the effect is due to an electronic perturbation of the metal function [2,4–6] (e.g., a charge transfer effect, as originally favoured by Tauster et al. [1,2]) or that it is due to encapsulation by some form of TiO_2 [8–10], which acts as a site blocker, a poison. A number of workers have shown that such encapsulation appears to happen, both by indirect meth-

* Corresponding author.
E-mail address: bowkerm@cf.ac.uk (M. Bowker).
[1] Present address: AWE Aldermaston, Berkshire, UK.
[2] Present address: Oxford Applied Research, Witney, Oxfordshire, UK.
[3] Present address: DeBeers, Ascot, Berkshire, UK.

0021-9517/$ – see front matter
doi:10.1016/j.jcat.2005.05.024

ods on single crystals [11–14] and by direct imaging [15, 16]. The elegant paper by Pesty et al. indicated fairly conclusively that the effect was due to encapsulation, although direct reactivity or adsorption studies were not carried out [11]. Their work was on model catalysts consisting of Pt nanoparticles deposited on single-crystal TiO_2(110). XPS indicated that an adsorbed layer of titania existed on the surface of the Pt, and that it was somewhat reduced, though the exact oxidation state could not be identified. It appears that the encapsulation model is now generally favoured [16].

Although much work has been carried out in relation to this phenomenon, and much has been surmised about the molecular-level events connected with it, the vast majority of this work is based on kinetic measurements on the macroscale. There have been very few investigations on the nanoscale in relation to this effect. There has been some HRTEM, which shows the migration of oxide species onto the metal component, but not the detailed atomic structure of the layer [15,16]. The model catalyst approach would seem to be a beneficial one in this respect, but very little work has been carried out in this direction. Some have worked with inverse catalysts of metal oxide films on single-crystal metals and have identified strong interactions [17–19], but it is not clear whether these closely relate to the SMSI effect on metal nanoparticles. An exception is the work of Diebold et al., who have examined possible nanostructures involved in these processes [20,21]. They used STM imaging of model Pt/TiO_2(110) catalysts to identify a new structure on the nanoparticles proposed to be due to a layer of only partly oxidised titania.

In this work we present a combination of kinetic, structural, and nanoscopic measurements aimed at obtaining a clearer impression of the SMSI effect with Pd as the reactive metal, since much less effort has been devoted to this system than to Pt, and because it is of interest to us in relation to photocatalysis. In particular the use of an STM that can operate in situ at high temperature at atomic resolution is an advantage in this respect and reveals the detailed structures that we believe are associated with the SMSI effect.

2. Experimental

The work described here was carried out on three different UHV machines. The kinetic work was carried out in a molecular beam reactor described in detail elsewhere [22]. This can be used to measure sticking probabilities, *S*, directly in the King and Wells fashion [23]. The XPS was carried out in a machine that also contained a LEED system (VG), a mass spectrometer, and facilities for metal vapour deposition and sputtering. Most experiments reported were carried out at normal exit of photoelectrons into the lens stack of the hemispherical analyser, but some were carried out at grazing exit (electrons emitted at 20° to the surface plane). The XPS comprised a VSW 100-mm hemispherical electron analyser with a single channeltron detector. In this work the source was Mg-K_α radiation produced by electron bombardment of the anode at a power of 240 W, and the analyser pass energy was usually 44 eV. The variable-temperature STM (WA Technology) has been described in detail elsewhere [24]. It can take images at up to 1000 K and has LEED/Auger, metal vapour deposition (MVD), and sputtering facilities. It has very good stability at high temperature such that movies (which require very low drift for good quality) have been taken at up to 1000 K [25].

The nanoparticles and films of Pd were formed by MVD with the sample held at 300 K. The source of Pd was a W filament tightly wrapped with Pd wire, which was resistively heated.

3. Results

3.1. Molecular beam studies

We have previously described the adsorption of CO on Pd/TiO_2(110) in detail [26], but Fig. 1 shows data for the effect of annealing temperature on the adsorption probability of CO at 300 K on a nanoparticulate model catalyst consisting of 12% coverage of Pd on TiO_2. The percentage of Pd is defined in terms of the CO uptake under the same conditions, in the same machine, on a pure Pd(110) crystal [27–29]. There is a huge decrease in the sticking probability and uptake after annealing to only 693 K, but the reduction of CO adsorption is even noticeable after annealing to only 633 K. The fundamental reasons for this reduction in adsorption efficiency are not evident from the molecular beam data, but clearly there has been a significant change in the surface properties of the model catalyst, and this drop in reactivity for CO parallels that seen for the SMSI effect [1,2] on powdered catalysts. It is known that sintering

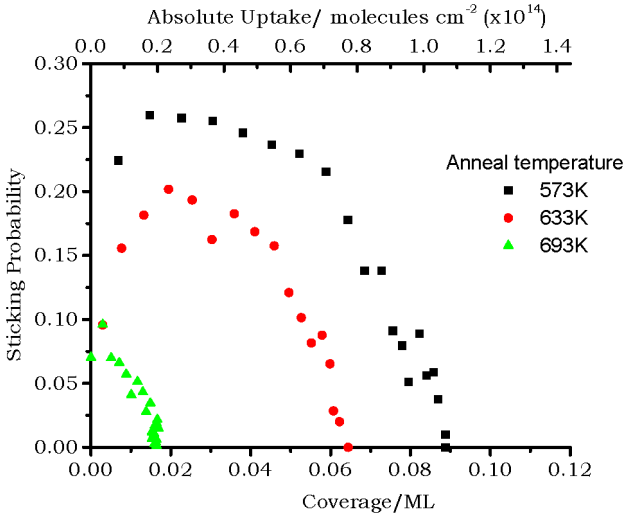

Fig. 1. Effect of annealing on the CO sticking probability, and its coverage dependence, measured using a molecular beam. The sample was a model catalyst of Pd nanoparticles on TiO_2(110) with 12% of the surface area covered by Pd.

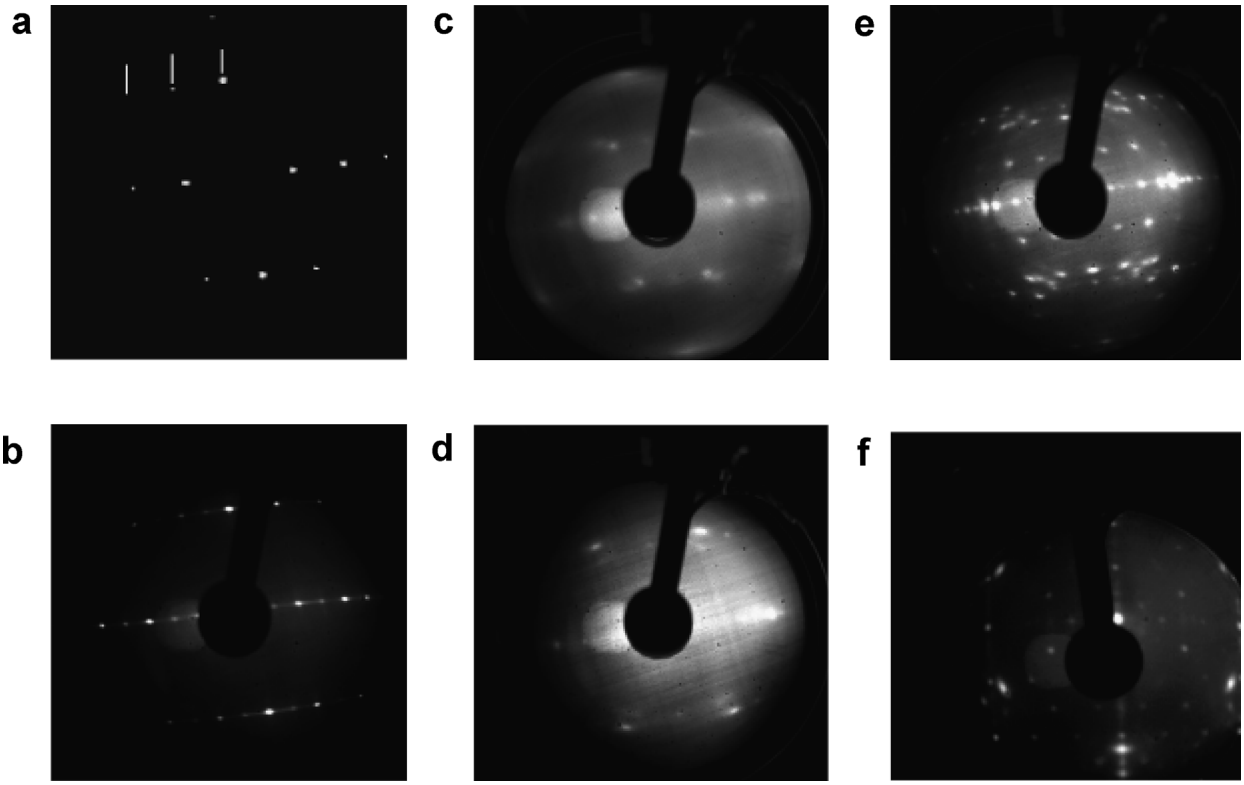

Fig. 2. LEED images taken for clean TiO_2(110) and during different stages of annealing the Pd film on TiO_2(110), all at 66 eV beam energy. (a) Clean TiO_2(110)-(1 × 1) surface. (b) Clean TiO_2(110)-(1 × 2) surface. (c) Hexagonal overlayer with a faint TiO_2(110)-(1 × 2) substrate pattern after annealing for 20 min at 573 K. (d) Hexagonal overlayer with a faint TiO_2(110)-(1 × 2) substrate pattern after annealing 20 min at 773 K. (e) Hexagonal overlayer with TiO_2(110)-(1 × 2) substrate pattern with sharp extra spots related to an overlayer formation after annealing for 20 min at 973 K. The pattern is assigned and explained in Fig. 9 and the associated text. (f) LEED pattern for an annealed Pd layer on a TiO_2(110) surface showing the c(6 × 2) structure due to surface contamination of the titania with Ca, together with the hexagonal Pd(111) pattern, which shows the broader spots.

is not significant for annealing the model catalysts at these temperatures [30,31]. In order to understand the causes of this activity decline, a range of techniques were used to examine the nature of the Pd/TiO_2(110) surface, as described in the following sections.

3.2. LEED

The evolution of the LEED pattern for the model catalysts depends somewhat on loading of the metal, and observations are difficult at very low loadings where the Pd particles are small and/or cover only a small part of the surface. The LEED observations here were made on a number of different model catalysts (both films and nanoparticles of Pd on TiO_2(110)) and were also carried out in all three vacuum systems described above, but were similar for all of the experiments. The observations can be summarised as follows for deposition on a TiO_2(110) surface: (i) Figs. 2a and 2b shows the two structures of the clean TiO_2 surface that are commonly observed, with the expected twofold symmetric pattern. (ii) After a film of Pd is dosed onto the (1 × 1) titania surface there is little change, except for an overall increase in background intensity and evidence of a very faint hexagonal pattern. (iii) After the surface is annealed to 500–800 K, a better-resolved hexagonal pattern is observed because of improved ordering of a Pd(111)-like adlayer (Figs. 2c and 2d). This is aligned in the [1–10] direction of the TiO_2 surface and shows the (111) surface parallel with the TiO_2 surface plane, as expected from other reports, for instance, that of Pesty et al. for Pt on TiO_2(110) [11]. (iv) Heating above this temperature produces a very complex LEED pattern with a large number of spots. This is shown in Fig. 2e, which is obtained from the Pd film after annealing to 973 K, when the pattern becomes sharper, though it begins to evolve at lower temperatures than that. Obviously, a significant change in the structure of the surface has taken place, and this is clarified by the STM reported below. The STM also aids us in interpreting the rather beautiful, but complicated LEED patterns and leads to the assignment of the spot pattern given below. Although not shown here, similar additional patterns were observed with a TiO_2-(1 × 2) initial surface structure (this structure is described in detail elsewhere [32]), or even in the presence of a contaminated titania surface layer showing the c(6 × 2)-Ca surface arrangement (Fig. 2f) [33,34], obtained when the crystal TiO_2 crystal had not been thoroughly bulk-cleaned of Ca contamination.

3.3. STM

Fig. 3 shows several STM images of the TiO_2 surface (in (1 × 1) and (1 × 2) arrangements, Figs. 3a and 3b) and of

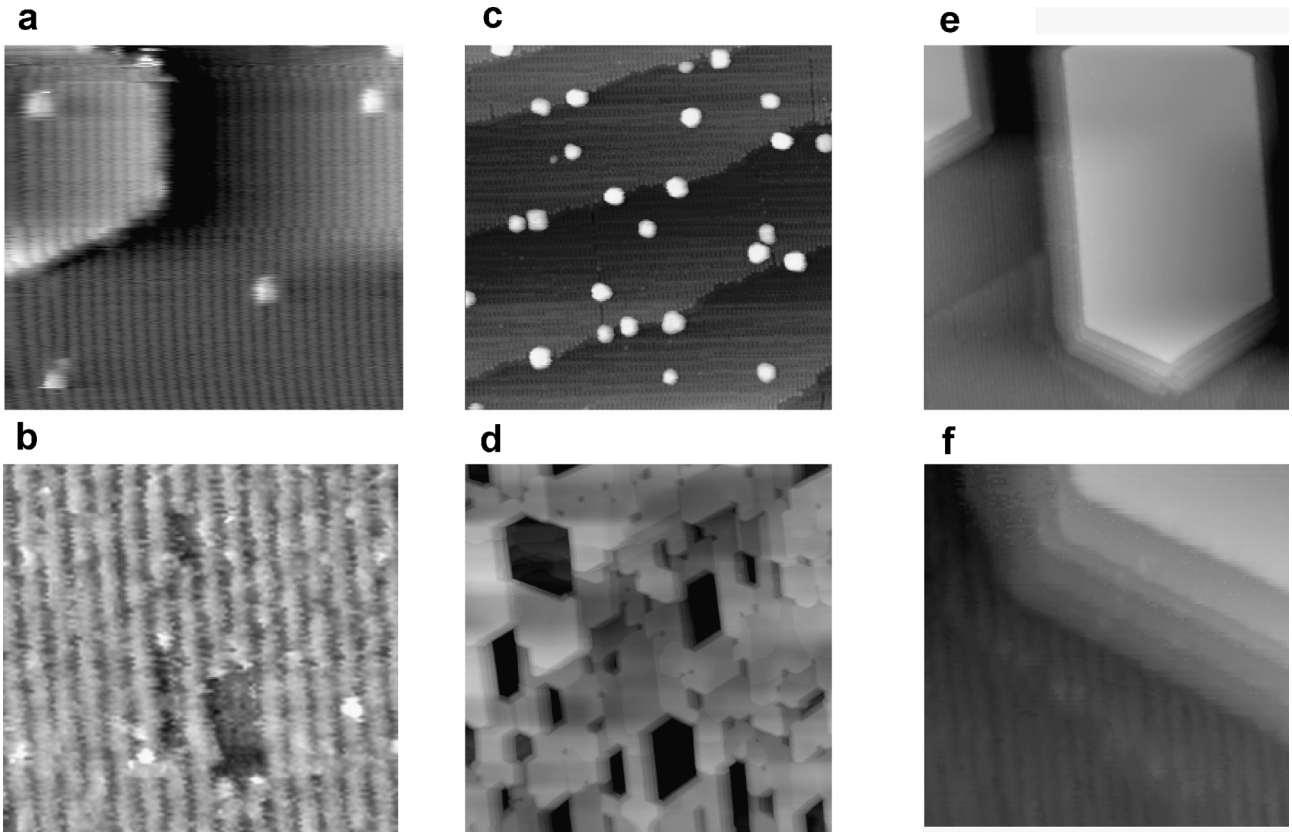

Fig. 3. STM images of the TiO_2(110) surface structures and various Pd overlayers (a) clean TiO_2(110)-(1 × 1) (19 × 19 nm); (b) clean TiO_2(110)-(1 × 2) (19 × 19 nm); (c) the surface covered with a low coverage of Pd in the form of small nanoparticles of ∼4 nm diameter (100 × 100 nm); (d) with a thick Pd film deposited, showing hexagonal holes down to the TiO_2 surface, (400 × 400 nm); (e) with large Pd nanoparticles, showing planar tops, after annealing to 973 K (100 × 100 nm); (f) detail of the nanoparticle shown in (e), revealing the planes of the Pd particle and the connection with the underlying (1 × 2) TiO_2 surface (25 × 25 nm).

the surface with a Pd film and with nanoparticles of various types. Depositing small amounts of Pd usually results in the formation of very small particles [29–31], as shown in Fig. 3c. These particles are impossible to image at atomic resolution because of their small size and the convolution of the particle and tip shape. Thus, for this work we used higher loadings of Pd on the surface, which results in the formation of Pd films or very large, flat-topped nanoparticles after annealing, as shown in Figs. 3d–3f. These particles are purposely large (∼10-nm diameter), so that they can be used to expose flat surfaces that can then be successfully imaged at atomic resolution by STM. We could not obtain imageable surface structures before high-temperature annealing, but after such treatment beautiful surface structures are observed (Fig. 4). It consists of two different types of surface domains: a zigzag structure (Figs. 4a, 4b and 4f) and a much more complicated arrangement that we call the “pinwheel structure” (Figs. 4a–4e), and these often coexist, as in Figs. 4a and 4b. The zigzag structure is very well ordered, often over large areas (Fig. 4f), but the pinwheel is much less well ordered, partly because of a much larger unit cell. Although there are several types of hexagonal patterns shown, we believe these all relate to a similar basic structure, as outlined below.

Although these structures are clearly resolved in STM, the composition of the surface layers is not directly accessible from these data. In order to clarify this aspect of the system, we have applied XPS to the analysis of these surfaces.

3.4. XPS

Similar surfaces were prepared in the XPS machine and verified by the use of LEED. Fig. 5 shows the effect of dosing Pd on the TiO_2 and Pd signals at both normal and grazing exits of the photoelectrons. Clearly the Ti signal decreases as the Pd increases, and at grazing exit the Pd/Ti ratio is very high. The loading here is very high at the end of this deposition, corresponding with about six layers of Pd. It is interesting to note that the small level of Ti^{3+} that is present in the sample in this case before Pd dosing (estimated to be ∼10% of total Ti signal) significantly decreases with Pd deposition to around 5%; this is a feature noted by others [35,36] and may relate to some initial nucleation of particles around surface defects, as described by Wahlstrom et al. for Au nanoparticles on TiO_2 [37]. Heating such a film results in a decrease of the Pd signal between 500–700 K (Fig. 6) and an increase in the titania signal. With the increase in

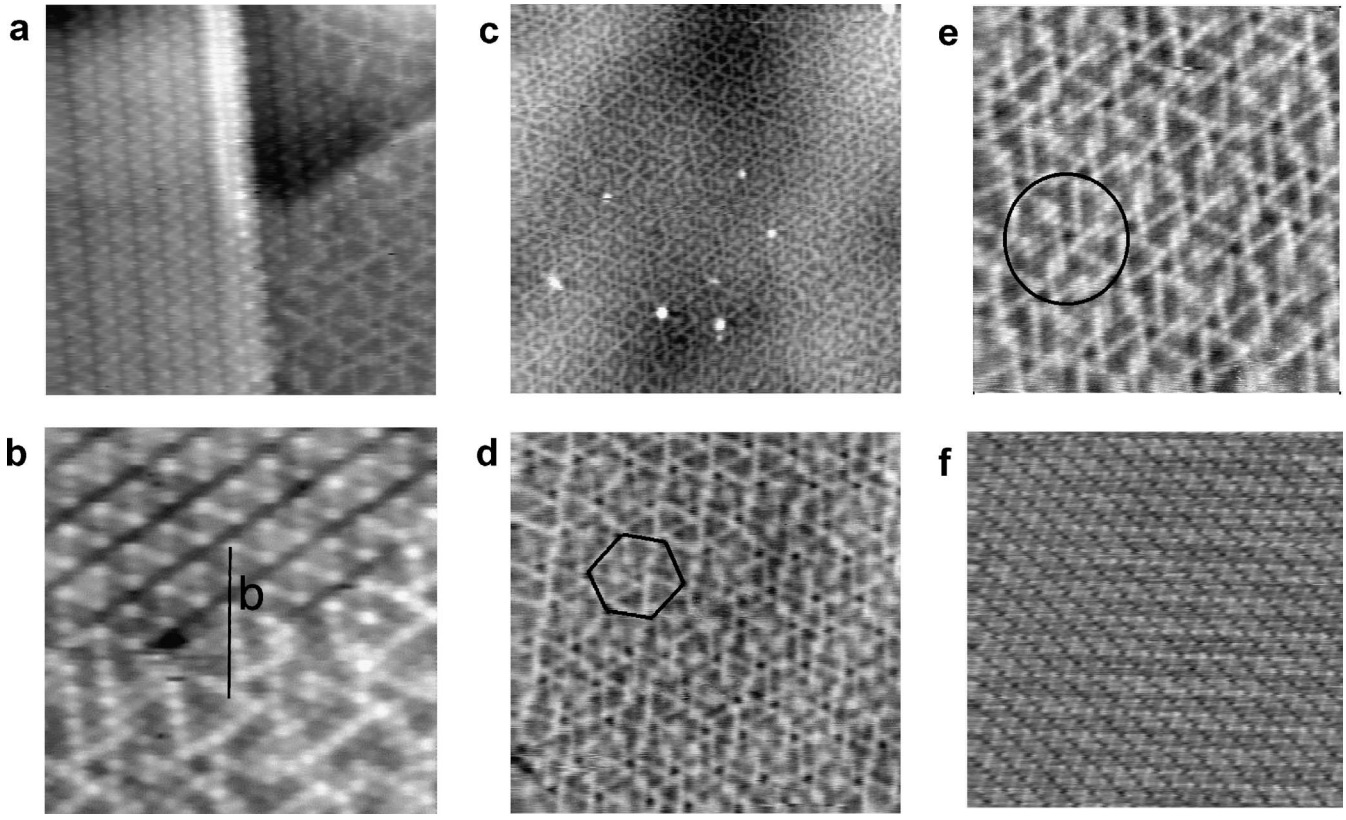

Fig. 4. STM images of the detailed surface structure of Pd nanoparticles and films after annealing to 973 K; (a), (b) and (f) from Pd films; (c), (d) and (e) from nanoparticles. Image sizes are: (a) 12.4 × 12.4 nm; (b) 5.8 × 5.8 nm; (c) 31.6 × 31.6 nm; (d) 15 × 15 nm; (e) 10 × 10 nm; (f) 20 × 20 nm.

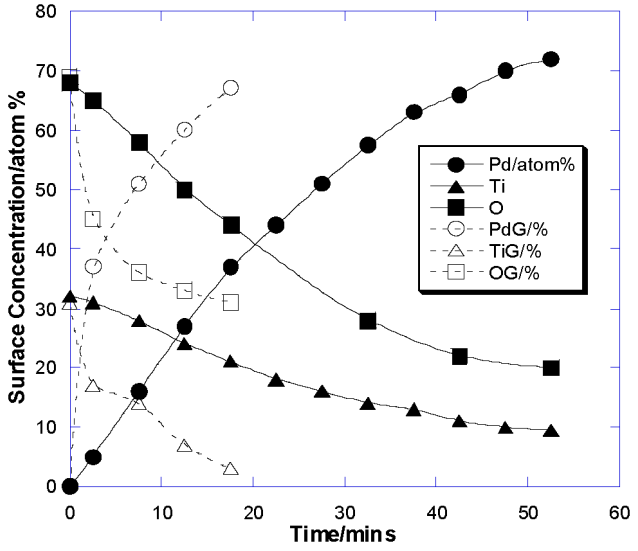

Fig. 5. XPS—the effect of Pd dosing on the Ti Auger signal with increasing Pd—taken at normal and grazing emission angles.

the Ti signal it is significant that the fraction of reduced Ti states in the XPS increases much more than does the Ti^{4+}, to a ratio of near equality. Some part of the loss of Pd signal at very high temperatures may due to sintering [30,31] and thereby to opening up of the TiO_2 surface to photoelectron escape from there, but this does not account for a number of other features of the data, especially the increase in the chemically reduced Ti states and the increase in Ti at relatively low temperature (below 673 K). The Ti signal ratio now changes little from normal to grazing incidence, and is high in the latter condition, in contrast to the results shown in Fig. 5.

It appears from the data of Fig. 6 that, at grazing exit, the Pd and reduced Ti signals increase, whereas Ti^{4+} and oxygen decrease. An example of the Ti XPS spectra at the two angles is shown in Fig. 7 and shows that after high-temperature annealing the surface is dominated at grazing exit by incompletely reduced Ti, and the 2p peaks appear at a significantly lower binding energy than for Ti^{4+}.

4. Discussion

It is clear from the data above that the change in reactivity of the surface for CO adsorption is associated with the changes in the surface structure and composition of the model catalyst that occur upon annealing. As the surface structure changes, so the reactivity diminishes, at least in terms of CO adsorption strength and sticking. This parallels previous observations of the type seen for the strong metal–support interaction SMSI [1–4].

A major question, then, is, what is the state of the metal surface during the SMSI process? It appears to be associated

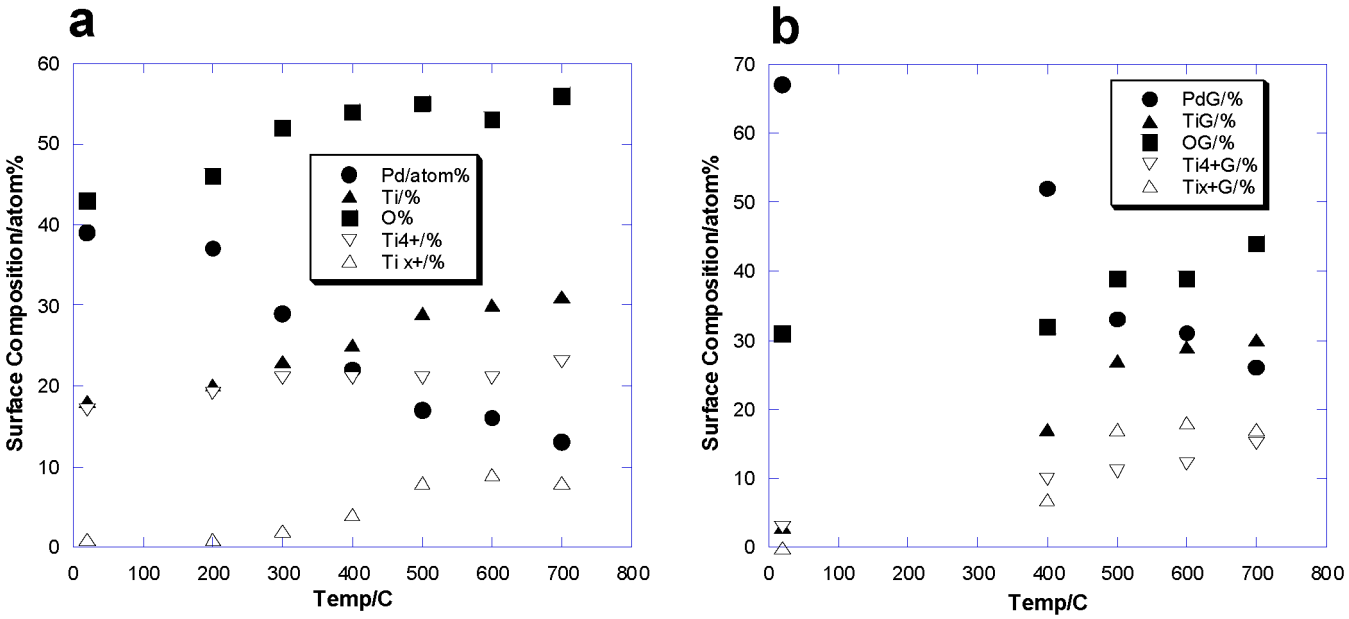

Fig. 6. XPS—the effect of heating a layer with approximately 3 monolayers equivalent of Pd deposited. Left hand panel—normal exit; right hand panel—grazing exit.

with the changes seen in the surface structure in STM and LEED and with the appearance of Ti in the Pd surface layers. This is evident from the significantly increased Ti signal, and decreased Pd signal, especially at grazing exit after annealing to only 673 K; the opposite behaviour with respect to the takeoff angle is seen in the XPS before annealing. This effect occurs because the Pd nanoparticles block the exit of electrons emanating from the TiO_2 into the analyser. The fact that after annealing the effect on the Pd/Ti ratio is reversed is sure evidence of Ti appearing in the surface layers of the Pd nanoparticles. Sintering alone does not explain the effect, since sintering has been shown previously to be insignificant below 700 K in a vacuum environment [30,31], and, furthermore, the Ti^{4+} fraction is lower at the grazing exit, whereas the Ti^{x+} is higher. Thus some kind of layer of titania forms on the surface of the Pd film and on the nanoparticles, as proposed by others in the past who used indirect methods (see, e.g., [8–10]). The SMSI is associated with the formation of this film and with the change in the surface which results. But what is the detailed nature of these changes?

The XPS results above indicate that the encapsulating Ti film is in a reduced state after annealing, but what state? We believe that it is not Ti^{3+}, because the shift from the Ti^{4+} peak seen in Fig. 7 is too large (∼3 eV to lower binding energy, whereas it should be ∼1.5 eV for Ti^{3+} [38]), and the peak is well separated from the Ti^{4+}. The shift seems comparable with that expected for Ti^{2+} (∼3.4 eV [38]). However, Bzowski and Sham report the binding energy for Ti^0 in a $PdTi_2$ alloy to be higher than that for Ti metal (which is at ∼453.8 (±0.3) eV), appearing at a binding energy of 455 eV [39], which they propose to be due to some charge donation from Ti to Pd, together with some intra-atomic

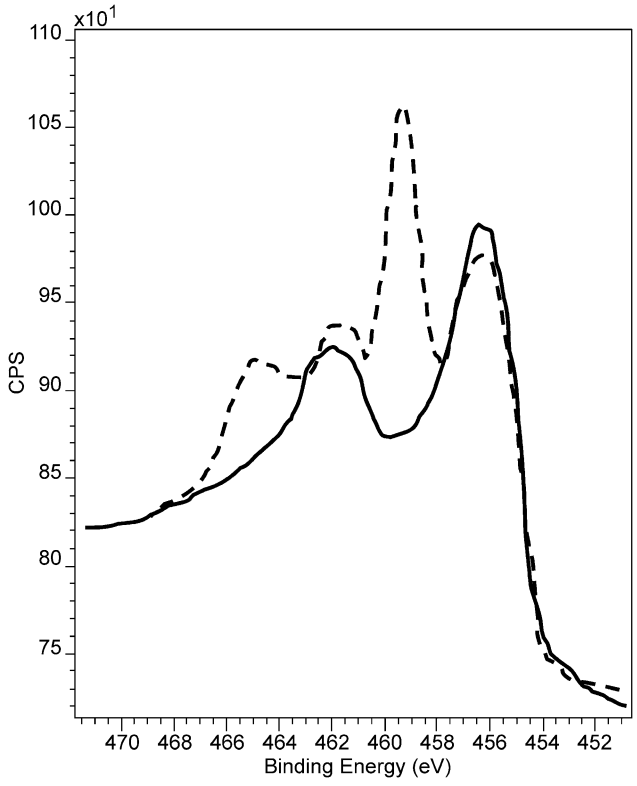

Fig. 7. XP spectra of a $Pd/TiO_2(110)$ surface with a high loading of Pd, annealed to 973 K at normal and grazing emission, showing both Ti^{x+} and Ti^{4+} at normal exit (---), but with much less Ti^{4+} apparent at grazing exit (—).

charge redistribution. Thus it could be possible that it is an alloyed form of titanium. The evidence to support the conclusion that it may be an oxide is the parallel increase in O(1s) XPS with the increase in reduced Ti, together with the

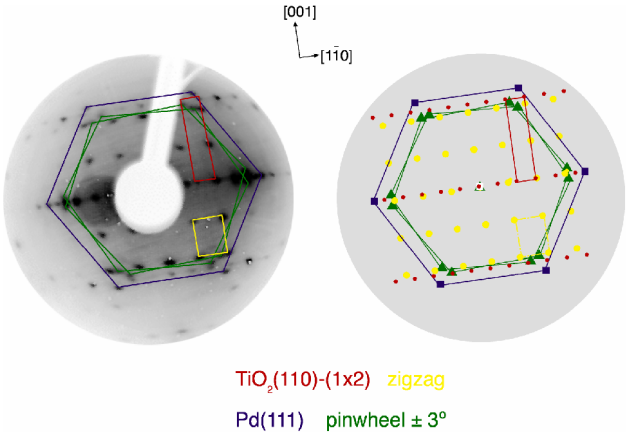

Fig. 8. Assignment of the LEED pattern shown in Fig. 2e. The four main structures are the substrate crystal TiO_2(110), the hexagonal Pd(111) pattern, and the two structures from the overlayer on the Pd, namely the zigzag and the pinwheel (the latter showing two slightly rotated domains).

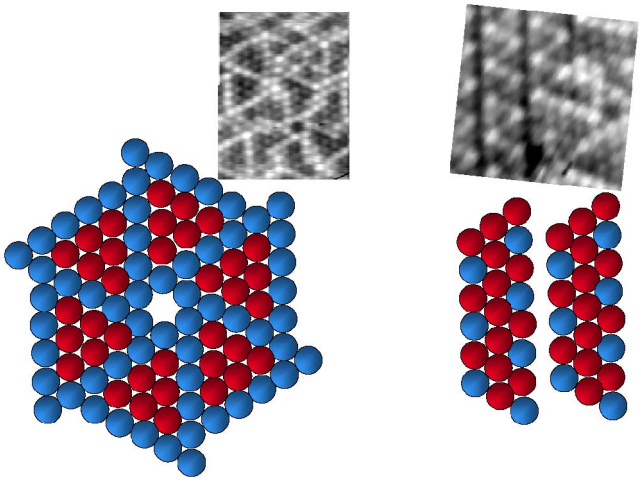

Fig. 9. Idealised surface structural models, together with the related high-resolution STM images.

loss in Ti^{4+} at the grazing exit (in Figs. 5 and 6). This is most likely to be due to the presence of reduced titania in the surface of the Pd nanoparticles, with the Ti^{4+} only present at the support oxide surface.

We now turn to the structural nature of the adlayer on the Pd. It is our contention that it is, at most, a thin layer on the surface of the Pd(111) nanoparticles, and most likely it is a single layer of changed composition. The reason for proposing this is that the underlying Pd(111) spots are usually clearly present in the LEED, as shown in Figs. 2 and 8. Fig. 8 shows an interpretation of the spot pattern of the LEED shown in Fig. 2e, which shows the same structures as seen in the STM images. Thus we can identify the twofold symmetric zigzag with the rectangular array of spots and the Pd(111) surface with the hexagonal set of spots. The pinwheel is proposed to be the slightly contracted hexagonal array of spots and occurs in two domains, rotated by ∼6° from each other, around the close-packed Pd direction. This explains the pattern and further gives us information about the directionality of the surface structures in relation to the underlying TiO_2 surface and of their relative size.

The proposed structure of these layers is presented in Fig. 9 and is at least partly conjectural. The zigzag is clearly seen in the STM, but of course this only identifies the unit cell and not necessarily all of the atoms in that unit cell. From the STM alone we are not clear which atoms are imaged, but it is not unreasonable to assume that tunnelling occurs into empty states of the surface at positive sample bias. Thus we assume that tunnelling occurs into metal/cation sites at the surface and that anions are not probed, as has been shown to be generally the case for titania [40,50]. Basically, the oxide atoms are assumed to be lacking empty states into which to tunnel. Thus the structures in Fig. 9 are presented as being composed of metal atoms. To go further, these atoms are distinguished in contrast, an effect often seen for alloy systems (see, for instance, [41]), which helps with the discrimination between the two atoms of the alloy and is associated with different effective local work functions and densities of states in the two atoms. We believe that the difference between the two structures, the zigzag and pinwheel, may be due to differing ratios of atoms in these two states, as shown in the figure; the details of the assignment of the atoms in the structure is given further below. Since we do not know the positions of the oxygen atoms, or their exact amount; these are not shown. Of course, if we assume that they are associated with Ti, and that, as indicated by XPS, the Ti is in the 2+ state, then each Ti atom may be associated with one oxygen atom. Since we do not identify clear black holes in the adlayer (except for the centre of the pinwheel), and since theorists show us that oxygen is usually imaged as a depression [42], then the oxygen could be at the interface between the Ti and the underlying surface. This is by no means certain, however; for the titania surfaces shown in Fig. 3, the Ti cations are imaged even though oxygen anions are the outermost atoms.

The only similar type of atomically resolved information is that reported by Diebold et al. [20,21] for Pt/TiO_2(110) model catalysts, but only the zigzag structure was observed in that case. There is, however, a significant difference between their zigzag structure and ours; a comparison of the two structures is shown in Fig. 10. The zigzag on the Pt nanoparticles has arms on the zigzag with five or six atoms imaged in them, whereas for Pd we have only three and have never seen any other size of zigzag, even over large areas, as shown in Fig. 4f. We believe this difference is due to a different mismatch between an overlayer present on top of the Pd(111) substrate compared with Pt(111). The lattice parameter of Pt is only slightly bigger than Pd (0.392 vs. 0.389 nm), and so it is hard to believe that a 1% difference could have such a drastic effect on the structure. This may be an indication that the lattice parameter for the surface atoms of the nanoparticles of the two metals on the titania surface is more different than it is for the pure metals themselves.

Jennison et al. attempted to model the Pt/TiO_2 zigzag structure theoretically [21]. They proposed that the oxygen

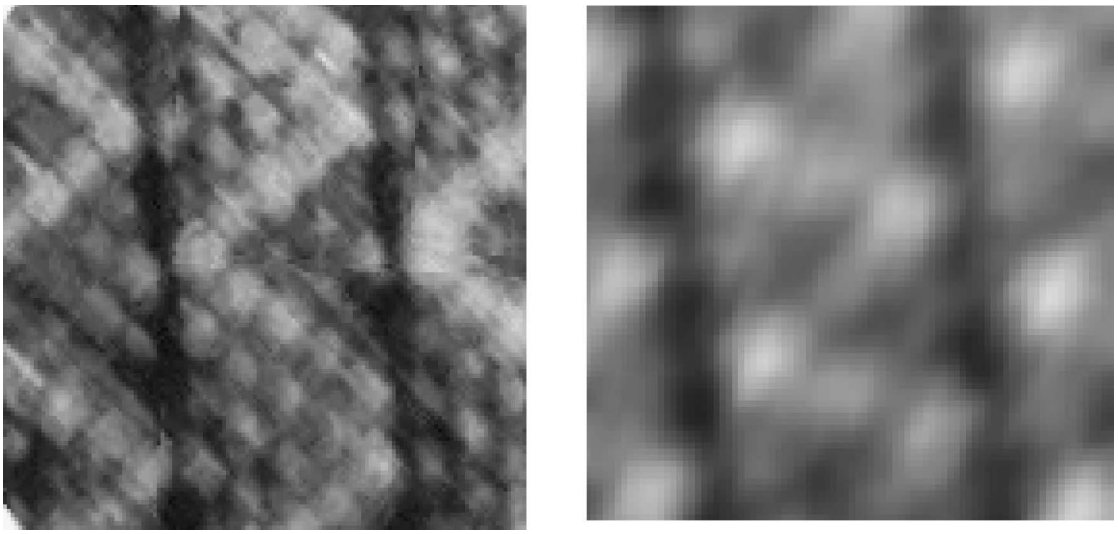

Fig. 10. Comparison of Diebolds zigzag image for $Pt/TiO_2(110)$ (left panel, 3.4 nm image) and ours for $Pd/TiO_2(110)$ (right panel, 1.62 nm image) at high magnification. For the former there are five atoms in the zigzag, but for ours there are only three.

lies on the top layer, though their proposed structure is in some ways much more complex than ours. A major difference between the two models is the nature of the surface layer; Diebold and Jennison favour what is essentially a surface bilayer of Ti–O on top of the Pt(111) surface. The difference between our two structures lies in the interpretation of the contrast difference in the structure. We explain the contrast as being due to the presence of two different metals in the adlayer, akin to the contrast seen for alloy systems by Varga et al. [41], whereas Diebold and Jennison consider it to be exclusively due to the mismatch between the surface and underlying layers. This may indeed be correct, but our reasons for disagreement with this model are given below, especially in relation to the pinwheel structure, where a similar contrast effect, like that for the zigzag, is also seen.

The pinwheel structure was not seen by Diebold et al. on nanoparticles, perhaps because it is not stable on the Pt nanoparticles, or perhaps because of limited data sets. It is obviously much more complex than the zigzag, but is related to it as shown in Figs. 4b and 9, where the two structures intermesh, apparently easily; both appear to be composed of locally close-packed, hexagonal surfaces. Furthermore, it is evident that the triangle formed by the zigzag contains the same number of atoms as the triangles within the spokes of the pinwheel (six atoms), although the composition appears to be different. If we consider the pinwheel structure in a little more detail, we can see that it appears to present the pinwheel motif, as shown in our model in Fig. 9. However, this motif is not actually the unit cell. The motif can be constructed from triangular, six atom-sided units, which intersect in a particular position in the triangle, as shown in Fig. 11a. If we extend this structure over a wider area, we can see that intersection with adjacent triangular units reveals the pinwheel motif as shown in Fig. 11b; this figure also shows the unit cell. The unit cell is a very large one, containing 25 atoms, which partly explains the difficulty the

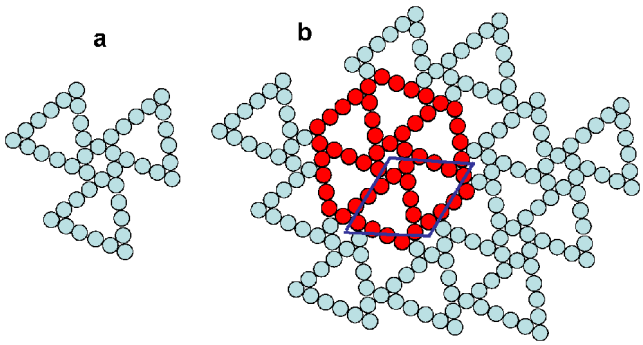

Fig. 11. Schematics of the pinwheel structure, showing its construction from the specific interlocking of three triangles with six atom sides, and showing the true unit cell.

system has in making completely regularly ordered arrays of this structure, as seen in Fig. 4. Note that, in contrast, the zigzag unit cell contains only six surface atoms.

What are the justifications for assuming that the pinwheel is constructed of different atoms? First of all, the contrast appears to be rather stark, with the radial arms of the pinwheel (the sides of the triangles in Fig. 11) being markedly brighter than the six atoms of the inner triangle. Earlier we attempted to explain this structure with a Ti-only termination (following Jennison et al.), as being due to varying position of the atoms with respect to the underlying Pd(111) surface [43]. However, such an approach does not easily explain the variations and mismatches seen in Fig. 4e for instance. In all of these images the arrangement of atoms seems to be essentially hexagonal, yet the triangles intersect badly in many areas. This would not be expected to be the case if the overlayer were all of one atom type, in a hexagonal arrangement, but could occur for insufficiently ordered mixes of atoms. Second, we would expect that at glancing exit, after annealing, the Pd signal would significantly decrease if it were encapsulated by titanium, whereas the *relative* amount of

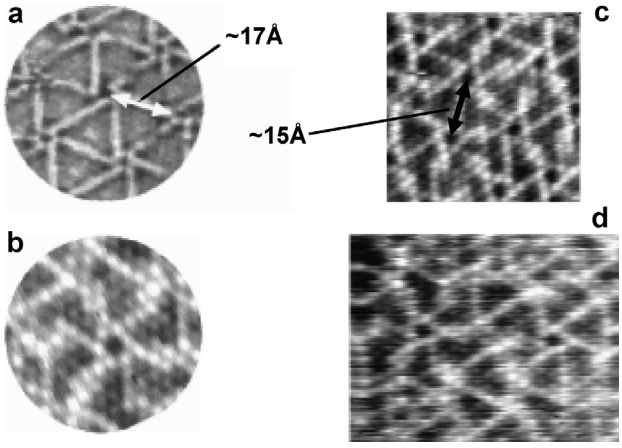

Fig. 12. A comparison of the images for the pinwheel structures of our Pd/TiO_2 model catalysts (b)–(d) and the Cr–Pt(111) surface alloy of Zhang et al. (a) [44,45].

Pd is higher at glancing exit (Fig. 6b). This suggests it is still in the outer layers. Finally, and most importantly, this structure is very similar to one found by Zhang et al. for a surface alloy system, namely, Cr deposited on Pt(111), followed by annealing [44,45]. This is shown in Fig. 12 to compare with some of our own images of the pinwheel structure, though atomic resolution was not quite obtained in the Zhang work. There is obvious similarity between the two, and Zhang et al. propose that the triangle centres of the pinwheel are composed of Cr, whereas the spokes are Pt, similar to our proposal for the current system. One point of difference is that for their structure Zhang et al propose a network of seven-atom-sided triangles, whereas we have six. There are some other detailed differences of structure that will be discussed elsewhere [46]. Since this is defined by Zhang et al. as a surface alloy system, this lends further justification to our proposal for the Pd/Ti system; essentially Ti takes the place of Cr in their model and Pd replaces Pt.

We choose to identify the brighter atoms as Pd, and the less bright are then Ti, the difference possibly being due to the presence of oxygen preferentially associated with Ti, due to the much higher affinity of the latter for oxygen (relative bond energies 670 $kJ\,mol^{-1}$ versus 380 $kJ\,mol^{-1}$ for Pd [47]). Further support for the latter idea is that oxygen desorbs rather easily from Pd (and is difficult to dissociate on the nanoparticles at low temperature when CO sticks well [29]), but not from TiO_2, the temperature for a significant desorption rate being ∼700 K from Pd crystals and much higher for TiO_2, and our surfaces have been annealed above 800 K. Indeed, it could be the case that the oxygen on the surface of the nanoparticles is adsorbed on top of the Ti—hence the low contrast of those atoms. Note that for TiO_2 itself (as shown in Fig. 3), Ti is imaged even though it is thought to be covered by oxygen atoms [48,49]. The Pd/Ti ratio in the pinwheel structure is then approximately 1:1. In the same way, then, we associate the bright atoms in the zigzag with Pd, meaning the surface layer has a Pd/Ti ratio of 1:2, as shown in Fig. 9.

It may be that this layer is a kind of surface intermetallic material. This could perhaps be why we have two structures of such well-defined atomic ratio; intermetallics are essentially stoichiometric compounds. It is interesting to note that some time ago Nuzzo and Dubois proposed that the SMSI effect was due to the formation of intermetallic compounds such as Pt_3Ti or Ni_3Ti [50], though we propose much more Ti-rich intermetallics than this. The bulk Pd–Ti phase diagram contains a range of well-defined phases of Pd–Ti, including PdTi and $PdTi_2$ [51]. Although intermetallic in nature, of course, it is the case that the Ti is also oxidised, and Nuzzo and Dubois note that this is generally the case for the intermetallics—the surface is easily oxidised.

If we return to the effect of SMSI on the adsorption of CO, we must note that a significant change already begins by 630 K, although total suppression does not occur until ∼730 K, a temperature very similar to that observed for the SMSI effect in powdered materials [1–6]. This is clearly in the region in which Ti segregation to the surface of the material begins as measured by XPS, but it is a little lower than the temperatures at which we observed good local ordering in STM, and a little lower than usually quoted for the effect in catalysis. It is likely then that even at 630 K, there is a titania layer of some sort at the surface of the Pd nanoparticles, but that is not present in a very ordered form at that stage. At the temperatures where the ordered surface layers form, the adsorption of CO, at 300 K surface temperature, is zero. SMSI reported in the literature is usually seen after heating to ∼800 K, in the region of the formation of the ordered surface layers.

Acknowledgment

The authors are grateful to a number of organisations for support for this work. This includes EPSRC for postdoctoral support to R.B., R.S., P.M., and M.H. under grants GR/L22584 and GR/R89882. They further provided a studentship for N.P. Johnson-Matthey are also acknowledged for support for N.P. via a Case award. E.F. was supported by both the University of Reading and by Cardiff University. We are grateful to the Royal Society for a fellowship to R.K.

References

[1] S.J. Tauster, S.C. Fung, R.L. Garten, J. Am. Chem. Soc. 100 (1978) 170.
[2] S.J. Tauster, S.C. Fung, J. Catal. 55 (1978) 29.
[3] S.J. Tauster, in: R. Baker, S. Tauster, J. Dumesic (Eds.), ACS Symp. Ser., vol. 298, ACS, Washington, DC, 1986, p. 1.
[4] S.J. Tauster, Acc. Chem. Res. 20 (1987) 389.
[5] E.I. Ko, R.L. Garten, J. Catal. 68 (1981) 223.
[6] D.E. Resasco, G.L. Haller, Stud. Surf. Sci. Catal. 11 (1982) 105.
[7] M. Bowker, P. Stone, R.A. Bennett, N. Perkins, Surf. Sci. 497 (2002) 155–165.
[8] D. Meriadeau, J. Dutel, J. Dufaux, C. Naccache, Surf. Sci. 97 (2002) 95.

[9] J. Santos, J. Phillips, J.A. Dumesic, J. Catal. 84 (1983) 147.
[10] G. Raupp, J.A. Dumesic, J. Phys. Chem. 88 (1984) 660.
[11] F. Pesty, H.-P. Steinruck, T. Madey, Surf. Sci. 339 (1995) 83.
[12] J. Pan, T.E. Madey, Catal. Lett. 20 (1993) 269.
[13] G. Poirer, B. Hance, J.M. White, J. Phys. Chem. 97 (1998) 5965.
[14] T. Suzuki, R. Souda, Surf. Sci. 448 (2000) 33.
[15] A. Logan, E. Braunschweig, A. Datye, Langmuir 4 (1988) 827.
[16] A. Datye, D. Kalakkad, M. Yao, J. Catal. 155 (1995) 148.
[17] P.L.J. Gunter, J.W. Niemantsverdriet, F.H. Ribeiro, G.A. Somorjai, Catal. Rev. Sci. Eng. 39 (1997) 77.
[18] A.B. Boffa, H. Galloway, P.W. Jacobs, J. Benitez, J. Batteas, M. Salmeron, A.T. Bell, G.A. Somorjai, Surf. Sci. 326 (1995) 80.
[19] G.A. Somorjai, C.M. Kim, C. Knight, ACS Symp. Ser. 482 (1992) 108.
[20] O. Dulub, W. Hebenstreit, U. Diebold, Phys. Rev. Lett. 84 (2000) 3646.
[21] D. Jennison, O. Dulub, W. Hebenstreit, U. Diebold, Surf. Sci. 492 (2001) L677.
[22] M. Bowker, Appl. Catal. 160 (1997) 89.
[23] D.A. King, M.G. Wells, Proc. Roy. Soc. London Ser. A 339 (1974) 245.
[24] M. Bowker, R.A. Bennett, S. Poulston, P. Stone, A. Jones, S. Haq, P. Hollins, J. Mol. Catal. 131 (1998) 185.
[25] P. Stone, R.A. Bennett, M. Bowker, New J. Phys. 1 (1999) 8; http://www.njp.org.
[26] M. Bowker, P. Stone, R.A. Bennett, N. Perkins, Surf. Sci. 497 (2002) 155.
[27] I.Z. Jones, R. Bennett, M. Bowker, Surf. Sci. 402 (4) (1998) 595.
[28] I.Z. Jones, R. Bennett, M. Bowker, Surf. Sci. 439 (1999) 235.
[29] N. Perkins, Ph.D. Thesis, University of Reading, 2001.
[30] R.A. Bennett, P. Stone, M. Bowker, Faraday Discuss. 114 (1999) 267.
[31] R.A. Bennett, P. Stone, M. Bowker, Catal. Lett. 59 (1999) 99.
[32] R.A. Bennett, P. Stone, N.P. Price, M. Bowker, Phys. Rev. Lett. 82 (1999) 3831–3834.
[33] O. Bikonda, C. Pang, C. Muryn, B. Daniels, S. Ferrero, E. Michelangeli, G. Thornton, J. Phys. B, in press.
[34] H. Norenberg, J. Harding, Appl. Surf. Sci. 142 (1999) 174.
[35] Y. Chung, W. Weissard, Phys. Rev. B 20 (1979) 3456.
[36] Z. Bastl, P. Mikusik, Czech. J. Phys. B 34 (1984) 989.
[37] E. Wahlstrom, N. Lopez, R. Schaub, P. Thostrup, A. Ronnau, C. Africh, E. Laegsgaard, J. Norskov, F. Besenbacher, Phys. Rev. Lett. 90 (2003) 0261011.
[38] NIST XPS database at https://srdata.nist.gov/xps/.
[39] A. Bzowski, T. Sham, Phys. Rev. B 49 (1993) 7836.
[40] U. Diebold, J. Anderson, K. Ng, D. Vanderbilt, Phys. Rev. Lett. 77 (1996) 1322.
[41] Y. Gauthier, R. Baudoing-Savois, J. Bugnard, W. Hebenstreit, M. Schmid, P. Varga, Surf. Sci. 466 (2000) 155.
[42] N.D. Lang, Phys. Rev. Lett. 56 (1986) 1164.
[43] R.A. Bennett, C. Pang, N. Perkins, R.D. Smith, P. Morrall, R. Kvon, M. Bowker, J. Phys. Chem. 106 (2002) 4688.
[44] L. Zhang, J. van Ek, U. Diebold, Phys. Rev. B 57 (1998) R4285.
[45] L. Zhang, J. van Ek, U. Diebold, Phys. Rev. B 59 (1999) 5837.
[46] M. Bowker, E. Fourre and M. Hall, in preparation.
[47] Handbook of Chemistry and Physics, twenty fourth ed., CRC Press, Boca Raton, FL, 1993.
[48] U. Diebold, Surf. Sci. Rep. 48 (2003) 74ff.
[49] U. Diebold, J. Lehman, T. Mahmoud, M. Kuhn, G. Leonardelli, W. Hebenstreit, M. Scmid, P. Varga, Surf. Sci. 411 (1998) 137.
[50] R. Nuzzo, L.H. Dubois, in: R. Baker, S. Tauster, J. Dumesic (Eds.), ACS Symp. Ser., vol. 298, ACS, Washington, DC, 1986, p. 136.
[51] J.L. Murray, in: T. Massalski (Ed.), Binary Alloy Phase Diagrams, Am. Soc. for Metals, Metals Park, OH, 1986, p. 1878.